American Mineralogist, Volume 68, pages 130–142, 1983

The crystal structure of a Li,Be-rich brittle mica: a dioctahedral–trioctahedral intermediate

JIUNN-CHORNG LIN AND STEPHEN GUGGENHEIM

Department of Geological Sciences
University of Illinois at Chicago
Chicago, Illinois 60680

Abstract

The crystal structure of a Li,Be-rich mica from Zimbabwe, intermediate in composition between the trioctahedral mica bityite-2M_1 [$Ca(LiAl_2)(AlBeSi_2)O_{10}(OH)_2$] and the dioctahedral mica margarite-2M_1 [$CaAl_2(Al_2Si_2)O_{10}(OH)_2$], has been studied by single crystal X-ray analysis ($R_1 = 0.030$, $R_2 = 0.031$) in space group Cc. On a statistical basis, the M(1) site (mean M(1)–O = 2.14Å) contains 0.55 Li and 0.45 vacancy, whereas the M(2) and M(3) sites (mean M(2)–O, = 1.902, M(3)–O = 1.903Å) are fully occupied by Al. In the tetrahedral sites, the ordering of Al,Be relative to Si is nearly complete (mean T–O: 1.723, 1.721, 1.632, 1.628Å) with a similar pattern to that found in margarite. This pattern violates the center of symmetry of the ideal space group $C2/c$. Such ordering is not environmentally induced and is a consequence of a more stable cation charge distribution. Hydrogen positions at ρ values of 22° and 58° are associated at each hydroxyl and indicate the effect on the O—H vector of vacancy and lithium substitutions in M(1), respectively. Apparent thermal parameters are explained by positional deviations of atoms between dioctahedral and trioctahedral regions. Generally, for all micas, the counter rotation of octahedral upper and lower oxygen triads in M(2) is related linearly to the difference in size of neighboring octahedra, and causes a small reduction in the lateral dimensions of the octahedral sheet. Octahedral flattening is most greatly affected by the field strength of neighboring octahedral cations, and less affected by either tetrahedral/octahedral misfit or the octahedral cation size.

Introduction

Bityite, $Ca(LiAl_2)(AlBeSi_2)O_{10}(OH)_2$, was described by Lacroix (1908) using material from Mt. Bity, Madagascar and again in 1947 by Rowledge and Hayton using impure material from Londonderry, Western Australia. Strunz (1956) gave X-ray powder and optical data of the Mt. Bity material. He found the structure to be a two layer modification and illustrated also the complex nature of the twinning found in this material. More recently, reported occurrences of bityite or micas of intermediate compositions between bityite and the dioctahedral mica, margarite-2M_1, $Ca(Al_2)(Al_2Si_2)O_{10}(OH)_2$, have been noted from the Middle Urals (Kutukova, 1959), three pegmatites in Zimbabwe (Gallagher and Hawkes, 1966), and a tin vein in Uganda (Gallagher and Hawkes, 1966). Unpublished data (Lin and Guggenheim) confirm that material from Pizzo Marcio, Val Vigezzo, Piemonte, Italy is lithium and beryllium rich also. Infrared data of material from Salisbury, Zimbabwe and Bikita, Zimbabwe have been presented by Farmer and Velde (1973).

Although early workers (*e.g.*, Holzner, 1936) have suggested that certain micas intermediate in composition may be composed of varying proportions of interleaved dioctahedral and trioctahedral layers, no such examples have been found. It is generally agreed that a complete simple solid solution series between dioctahedral and trioctahedral micas (where an octahedral cation substitutes for a vacancy) does not appear to exist in nature, although it has been documented in synthetic systems (Toraya *et al.*, 1978a). Cases do exist in nature when the vacancy is ordered in the M(1) site (for example, lepidolite-2M_2 as refined by Takeda *et al.*, 1971) but cations are disordered over the other octahedral sites, thereby discounting a simple solid solution relationship between two end members. However, bityite represents a special case for sev-

0003–004X/83/0102–0130$02.00

eral reasons. Aluminum is known to strongly prefer the M(2) site in the micas and because of the coupled substitution of Be for Al in the tetrahedral sites, a simple Li substitution for the vacancy is possible without additional octahedral substitutions or octahedral cation disordering effects. Furthermore, the ionic radius of lithium is nearly the same size as the vacancy in aluminian dioctahedral micas. Thus, the topology of the octahedral sheet of bityite would be similar to that of an aluminian dioctahedral mica if lithium substitutes for the vacancy.

The distribution of tetrahedral cations is of interest also. Margarite-$2M_1$ has been shown to adopt a nearly complete ordered arrangement of Si and Al in a pattern that violates the center of symmetry (Guggenheim and Bailey, 1975). Because of the similarities of the margarite and bityite structures and chemistry, a similar ordering pattern would be expected for bityite. Infrared data (Farmer and Velde, 1973) appear to confirm that intermediate members of the series are ordered based on spectra suggesting the absence of Al–O–Al bonds linking tetrahedra. In addition, second harmonic laser studies (Guggenheim *et al.*, in prep.) indicate acentricity.

A single crystal X-ray refinement of the structure of a Li,Be mica has been undertaken on a sample from the Mops pegmatite, Salisbury district, Zimbabwe. The material replaces portions of a beryl crystal and is either a late stage magmatic or a hydrothermal alteration product. The optical properties are similar to that of margarite but with refractive indices of $\alpha = 1.639$, $\beta = 1.648$ and $\gamma = 1.650$ (Gallagher and Hawkes, 1966).

Experimental

Table 1 presents the wet chemical analysis (Gallagher and Hawkes, 1966) of crushed material from the Mops pegmatite, Zimbabwe. In addition, four grains from the same sample fraction were analyzed with a MAC5 three spectrometer automated electron microprobe using RAP (for Al) and PET (for Si and Ca) crystals. Up to six analyses per grain were made using standards from the Smithsonian Institution (hornblende, Kakanui, New Zealand and anorthite, Great Sitkin, Alaska). Grains analyzed using both standards separately produced comparable results. Similar results were obtained from the different crystals analyzed and individual crystals appeared homogeneous. The data were corrected using the Bence and Albee (1968) method and the alpha values of Albee and Ray (1970). The excess silicon reported in the wet chemical analysis is undoubtedly due to the observable presence of closely intergrown anhedral quartz (Gallagher and Hawkes, 1966). The amount of excess quartz may be calculated by comparing the wet and probe Al_2O_3 and CaO data; approximately 8% of the sample used in the wet analysis was due to included quartz. Appropriate adjustments were made to compensate (see Table 1) and the "best" data for all elements are given.

A crystal, approximately $0.25 \times 0.175 \times 0.05$ mm in size, was chosen from the split of crushed analyzed material. The crystal, mounted on the fiber along the c^* axis, gave only sharp reflections indicating regular stacking. Precession photographs showed monoclinic symmetry with systematic absences of the type $h + k \neq 2n$ for general reflections and $l \neq 2n$ for $h0l$ reflections. Models examining the possible adoption of symmetry in $C2/c$ and Cc were investigated.

Data were collected on a Picker FACS-1 four circle automated diffractometer using a graphite monochrometer and molybdenum radiation. Nineteen high-angle reflections in which $K\alpha_1$ could be re-

Table 1. Chemical analysis of the Li,Be mica from Mops Pegmatite, Zimbabwe

Oxide	[1]Wet	Probe	[5]Best	Cations per 22 positive charges		
SiO_2	36.1	31.26	31.26	Si	2.023	
BeO	3.8	[3]na	4.1	Be	0.637	4.000^{IV}
Al_2O_3	40.8	44.37	44.37	Al	1.340	
Li_2O	1.9	na	2.1	Al	2.044	
Fe_2O_3	0.02	[4]0.17	0.17	Li	0.547	2.598^{VI}
TiO_2	0.2	bd		Fe^{3+}	0.007	
MgO	0.1	bd				
CaO	12.7	13.64	13.64	Ca	0.946	
Na_2O	0.4	0.19	0.19	Na	0.024	0.971^{XII}
K_2O	0.1	0.008	0.008	K	0.001	
H_2O	4.7	na	5.1			
F	[2]bd	na				
	100.8	89.64	100.94			

1. from Gallagher and Hawkes (1966)
2. below detection
3. not analyzed
4. all iron assumed ferric
5. BeO, LiO and H_2O of wet analysis multiplied by 1.081 to account for quartz contaminant (see text).

solved were used to refine the unit cell parameters (see Table 2). Intensity data were collected using the moving crystal, stationary counter technique in the continuous ω scan mode (Lenhert, 1975) at 1°/min scan, 1.5° peak width and a 20 sec. per background count. Intensity measurements in one half of the reciprocal sphere were collected to produce 7914 reflections with limitations of $h = -10$ to 10, $k = -17$ to 17 and $l = 0$ to 37 and Sin $\theta/\lambda = 1.0$. Crystal and electronic stability were monitored by comparing a set of three standard reflections taken after every 50 observations. The data were corrected for Lorentz and polarization effects. Corrections for absorption effects were calculated empirically based on ψ scans (10° increments in ϕ) for selected reflections taken at approximately 5° intervals in 2θ. A comparison of ψ scan data showed that the maximum intensity decrease was 24%.

Only reflections in which $I > 3\sigma(I)$ were considered observed where the standard deviation, σ, of the intensity, I, is defined as $\sigma(I) = [c + 0.25(t_c/t_b)^2(B_1 + B_2) + (pI)^2]^{1/2}$; c is the total integrated counts in time t_c, B_1 and B_2 are the background counts in time t_b, and p is arbitrarily chosen as 0.03 and $I = [c - 0.5(t_c/t_b)(B_1 + B_2)]$. These reflections were symmetry averaged into two quadrants resulting in 1927 non-zero, independent intensities. Ten reflections were removed from the data set because of difficulties encountered in translating the paper tape.

Refinement

The atomic coordinates from margarite in the ideal space group, *C*2/*c*, were used as the initial model for refinement in the crystallographic least-squares program, ORFLS (Busing, Martin and Levy, 1962). The use of this model implies silicon and aluminum (and beryllium) disorder in the tetrahedral sites. Scattering factor tables were from Cromer and Mann (1968), atoms were assumed to be half ionized, and reflections were given unit weights. As a first step, the M(1) site was left vacant as is typical in dioctahedral micas. A three dimensional Fourier difference map was generated after several cycles of varying atomic coordinates followed by varying isotropic temperature factors. A positive anomaly, approximately 1 1/4 e/Å^3, was detected at M(1). Since the calculation of bond distances showed complete ordering of Al in M(2), the entire electron density at M(1) was attributed to all the octahedral elements in excess of two Al ions, predominantly lithium. Additional cycles involved varying the isotropic temperature factor of M(1) and the anisotropic temperature factors and atomic coordinates (see Table 3) of the remaining atoms. A second Fourier difference map was computed after these cycles and the hydrogen positions located (see the discussion below). No other significant features were found. The final residual values are given in Table 4. Bond lengths calculated at this stage confirmed the assumptions made earlier regarding tetrahedral disorder in *C*2/*c* symmetry.

Table 2. Unit cell parameters of the Mops mica compared to margarite

	Li, Be mica	[1]Margarite
a (Å)	5.058(1)	5.1038(4)
b (Å)	8.763(3)	8.8287(7)
c (Å)	19.111(7)	19.148(1)
β (°)	95.39(2)	95.46(3)

[1]from Guggenheim and Bailey, 1975

Refinement procedures in *Cc* symmetry follow the method outlined by Guggenheim and Bailey (1975, 1978) and summarized by Guggenheim (1981). In short, it involves the testing of each artificially ordered model with atomic coordinates derived by a *distance* least-squares program in the lower symmetry. *X*-ray intensities are then used for each model in a full-matrix least-squares refinement program. The ordered model as found in margarite (Si in T(11) and T(2), Al in the other tetrahedral sites) is the only ordering scheme which does not segregate Al and Si into separate tetrahedral sheets but is still consistent with a disordered arrangement in *C*2/*c* symmetry. Because of the two layer stacking sequence and the *c* glide plane, the "converse" model of silicon in T(1) and T(22) may be made congruent to that of the margarite structure by rotation and an origin shift. The effect of Be on the starting model was considered too subtle to require modelling since statistically, if complete ordering of Be occurs, only one half of a Be atom can occupy one tetrahedral site.

The calculation of bond lengths at the end of the isotropic refinement in *Cc* symmetry showed the Al-rich tetrahedra to be smaller than in margarite. A Fourier difference map indicated also that the scattering power in these sites should be less and the scattering factor tables were adjusted (to 9.5 and 9.1

Table 3. Atomic coordinates for the Mops mica

	C2/c Refinement				*Cc* Refinement									
Atom	x	y	z	[1]$B_{eq.}$	x	y	z	$B_{eq.}$	β_{11}	β_{22}	β_{33}	β_{12}	β_{13}	β_{23}
Ca(1)	0.0	0.0911(1)[2]	0.25	1.08	0.0	0.09104(9)	0.25	1.18(2)	0.0136(2)	0.00485(6)	0.00045(1)	-0.0004(3)	0.00029(3)	-0.00010(7)
M(1)	0.25	0.25	0.50	3.2(5)	0.259(6)	0.248(4)	0.503(2)	1.1(2)						
M(2)	0.2538(2)	0.0841(1)	0.00005(5)	0.37(1)	0.7458(7)	0.9152(3)	0.9999(2)	0.38(6)	0.0038(6)	0.0012(2)	0.00025(4)	0.0006(2)	-0.0000(1)	-0.00003(5)
M(3)					0.2535(7)	0.0847(3)	0.0000(2)	0.44(6)	0.0035(6)	0.0017(2)	0.00030(4)	-0.0006(2)	0.0003(1)	0.00005(6)
T(1)	0.4657(2)	0.9237(1)	0.14373(5)	0.46(1)	0.4653(8)	0.9238(4)	0.1421(2)	0.75(8)	0.0052(8)	0.0039(3)	0.00036(5)	-0.0016(4)	0.0001(2)	0.0004(1)
T(11)					0.5346(6)	0.0768(2)	0.8552(1)	0.24(4)	0.0042(5)	0.0004(1)	0.00011(3)	0.0008(2)	0.00014(9)	-0.00011(5)
T(2)	0.4567(2)	0.2541(1)	0.14370(4)	0.48(1)	0.4575(6)	0.2535(3)	0.1443(2)	0.52(3)	0.0039(5)	0.0031(2)	0.00015(3)	-0.0007(3)	-0.00002(8)	0.00011(7)
T(22)					0.5436(7)	0.7450(3)	0.8572(2)	0.37(6)	0.0055(7)	0.0003(2)	0.00032(4)	0.0009(4)	0.0001(1)	0.00004(9)
O(1)	0.9557(4)	0.4374(2)	0.0558(1)	0.60(3)	0.958(1)	0.4397(5)	0.0517(2)	0.43(9)	0.005(1)	0.0020(3)	0.00012(5)	0.0013(4)	0.0002(2)	0.0001(1)
O(11)					0.046(1)	0.5648(6)	0.9402(2)	0.47(9)	0.004(1)	0.0028(3)	0.00010(5)	0.0005(4)	0.0002(2)	0.0003(1)
O(2)	0.3961(4)	0.2514(2)	0.05589(9)	0.55(2)	0.400(1)	0.2520(6)	0.0582(2)	0.53(9)	0.007(1)	0.0016(3)	0.00027(5)	0.0006(5)	-0.0003(2)	-0.0001(1)
O(22)					0.610(1)	0.7492(6)	0.9467(2)	0.46(9)	0.006(1)	0.0011(3)	0.00030(5)	-0.0006(5)	0.0002(2)	0.0002(1)
O(3)	0.3592(4)	0.0871(3)	0.1760(1)	0.75(3)	0.362(1)	0.0927(6)	0.1750(3)	0.9(1)	0.009(1)	0.0033(5)	0.00042(8)	0.0014(6)	0.0001(3)	0.0004(1)
O(33)					0.642(1)	0.9172(5)	0.8231(3)	0.6(1)	0.007(1)	0.0013(3)	0.00046(7)	-0.0015(5)	0.0013(3)	-0.0001(1)
O(4)	0.2814(4)	0.7773(2)	0.1678(1)	0.69(3)	0.275(1)	0.7753(6)	0.1671(2)	0.8(1)	0.007(1)	0.0038(5)	0.00040(7)	-0.0006(6)	-0.0004(2)	0.0001(2)
O(44)					0.714(1)	0.2208(6)	0.8313(2)	0.6(1)	0.006(1)	0.0016(4)	0.00054(8)	0.0001(5)	0.0001(2)	0.0005(1)
O(5)	0.2804(4)	0.3933(2)	0.1772(1)	0.69(3)	0.291(1)	0.3902(6)	0.1760(3)	0.6(1)	0.005(1)	0.0029(4)	0.00036(7)	0.0014(5)	-0.0002(2)	0.0000(1)
O(55)					0.730(1)	0.6034(6)	0.8225(3)	0.6(1)	0.005(1)	0.0022(4)	0.00044(7)	0.0007(5)	-0.0004(2)	-0.0004(1)
[3]O(6)	0.4499(4)	0.5674(3)	0.0503(1)	0.61(3)	0.449(1)	0.5704(6)	0.0495(3)	0.6(1)	0.002(1)	0.0033(4)	0.00031(8)	0.0002(6)	-0.0002(2)	-0.0004(2)
O(66)					0.550(1)	0.4345(6)	0.9490(3)	0.6(1)	0.008(1)	0.0013(3)	0.00041(9)	-0.0017(6)	0.0011(3)	-0.0000(1)

[1] $B_{eq.}$ is calculated from $4/3[\beta_{11}/(a^*)^2+\beta_{22}/(b^*)^2+\beta_{33}/(c^*)^2]$. The anisotropic temperature factor form is $\exp(-\Sigma_i\Sigma_j\beta_{ij}h_ih_j)$.

[2] Values in parenthesis represent estimated standard deviations (esd) in terms of the least units cited for the value to the intermediate left, thus 0.0911(1) indicates an esd of 0.0001.

[3] Equal to OH.

Table 4. Results of refinement

	In *C2/c*		In *Cc*		
	Anisotropic		Isotropic		Anisotropic
[1]R	0.045	0.138	0.052	0.132	0.030
[2]wR	0.054	0.302	0.051	0.262	0.031
[3]goodness-of-fit	1.84	0.02	1.75	0.01	1.08
variable parameters	88	88	76	76	174
[4]data set	1917	3492	1917	3492	1917

[1] $R_1 = (\Sigma||Fo|-|Fc||)/\Sigma|Fo|$

[2] $wR = \{[\Sigma w(|Fo|-|Fc|)^2]/\Sigma w|Fo|^2\}^{\frac{1}{2}}$; for the data set of 1917 reflections, w=1; for the data set of 3492 reflections, if $F \geq 10$, then $w=1/(\sigma xF^2)$; if $F < 10$, then $w=1/(\sigma x10xF)$ and if F=0, then $w=1/(163x10)$ where 163 is the σ of the weakest non-zero reflection. The total number of reflections for $F \geq 10$ is 1859. See text for significance.

[3] Goodness-of-fit: $[\Sigma w||Fo|-|Fc||^2/\Sigma(n-m)]^{\frac{1}{2}}$ where n=number of independent data and m=number of parameters.

[4] Complete data set: 3492; Data set for which $I>3\sigma$ considered observed: 1917.

electrons/Å^3) to include Be. No significant differences were found between the two Al,Be-rich tetrahedra. The anisotropic refinement proved successful and, after a Fourier difference map was calculated, the hydrogen positions were located, although not included in the refinement.

Correlation coefficients in *Cc* symmetry are comparable to those observed in the margarite refinement and may be grouped into three classes. The highest correlations, from |0.900| to |0.956|, result generally from parameter interactions between M(2) and M(3) and between the *x* parameters of pseudosymmetry-related tetrahedral cations. Correlations from |0.850| to |0.900| involve interactions between the other parameters of the pseudosymmetry-related tetrahedral cations and the *x* parameters of pseudosymmetry-related anions, and those correlations below |0.850| involve the other variables. The latter class of correlations were mostly near zero. Higher correlations involving interactions for the *x* parameter and, consequently, the higher standard deviations associated with the positional parameters are probably related to the relatively lower values of the *h* index for reflections in the data set.

A comparison of the weighted residual for the anisotropic *C2/c* refinement and the isotropic *Cc* refinement shows that the latter refinement involving fewer variables has a significantly lower value. The difference increases substantially (Table 4) if a data set is used in which weak and zero reflections are emphasized. These reflections are proportionally more greatly affected by the small imaginary component of the structure factor in a noncentric structure than the more intense reflections (Schomaker and Marsh, 1979). For this case, such a test is quite appropriate because the phases for the weaker $k \neq 3n$ reflections tend to be controlled by those atoms that do not repeat at *b*/3 intervals, *i.e.* the oxygen atoms, which deviate more from centrosymmetry. These results and the conclusions independently derived from infrared data and the SHG experiments indicate that the correct space group is *Cc*.

Table 5[1] lists the observed and calculated structure amplitudes and Table 6 gives the calculated bond lengths and angles. Values in Table 6 were

[1]To receive a copy of Table 5, order Document AM-83-213 from the Business Office, Mineralogical Society of America, 2000 Florida Avenue, N.W., Washington, D.C. 20009. Please remit $1.00 in advance for the microfiche.

calculated from ORFEE (Busing *et al.*, 1964) using the correlation coefficients.

Discussion

Giese (1979) has defined the hydrogen bond angle, ρ as the angle between the O—H vector and (001) as measured with respect to the M(1) site. For margarite, which has a vacant M(1) site, Giese predicts that ρ is small and the hydrogen vector nearly parallel to the (001) plane. Although both the interlayer cation and the complete occupancy of Li in M(1) for end member bityite would affect the hydrogen position in a complex way, one would predict qualitatively that the hydrogen vector is substantially elevated from the (001) plane relative to margarite because of the associated charge in the M(1) site of bityite. The final Fourier difference maps for both *C*2/*c* and *Cc* models suggest two plausible hydrogen locations near each hydroxyl position. We designate these peaks as H_L for low and H_H for high elevations relative to M(1) and the (001) plane. The locations of these peaks in *Cc* symmetry are: $H(1)_H$: 0.456, 0.638, 0.044; $H(1)_L$: 0.404, 0.642, 0.064; $H(11)_H$: 0.540, 0.370, 0.908; and $H(11)_L$: 0.592, 0.362, 0.938.

The hydrogen peaks designated H_L are the strongest peaks in the difference map at approximately 0.28 e/Å^3. The H_H positions are associated with peaks of 0.18 e/Å^3 in magnitude and are similar in value to peaks associated with atom positions. These latter peaks near atom positions suggest that the "thermal" ellipsoids incompletely describe the atomic thermal vibrations. Peaks apparently associated with random background effects are slightly lower in magnitude. We note, however, that the standard deviation for peak height in the difference map (Lipson and Cochran, 1950, p. 334) is 0.12 e/Å^3, and the conclusions regarding hydrogen peak positions should be considered tentative.

Observed values of ρ in *Cc* symmetry are (low and high, respectively) 23.2° and 57.3° for H(1) and 19.8° and 58.8° for H(11). The O—H distances are H(1): 0.73Å and H(11): 0.71Å for H_L, and H(1): 1.04Å and H(11): 0.97Å for the H_H positions. These distances involve an *average* associated oxygen position; the actual position of the oxygen is dependent on the occupancy of M(1), either a lithium ion or a vacancy. The average distance of 0.86Å compares favorably to O—H distances derived from other X-ray refinements. The multiple locations for the hydrogen position near each associated oxygen position emphasize that the crystal is composed of dioctahedral (Li-poor) and trioctahedral (Li-rich) unit cells. Except for the hydrogen position, which must differ considerably in lithium-rich or lithium-poor unit cells, the other atom coordinates represent average positions. Such average positions would be expected to influence the thermal parameters, which are described and discussed below.

There is no significant positional difference for the M(1) site *between* the ideal (*C*2/*c*) and subgroup (*Cc*) refinements. Neither the *R* value nor the isotropic temperature factor changed appreciably when, at the end of the refinement procedure in *Cc* symmetry, the positional parameters were re-set artificially to the ideal *C*2/*c* Wyckoff position of ¼¼½. In addition, estimated standard deviations for the positions of this site at the end of the refinement procedure are less than 3σ from the ideal position. However, the bond lengths and angles given in Table 6 are calculated using the refined position.

Figure 1 gives a polyhedral representation of the structure projected down the *a* axis and Figures 2 and 3 illustrate polyhedral structural components projected on (001). The octahedral cations (Fig. 2) are ordered with M(1) being larger than M(2) as is normal for most micas. The mean M—O,OH bond lengths (M(1), 2.14Å; M(2), 1.902Å and M(3), 1.903Å) are in good agreement with calculated values (M(1), 2.148Å; M(2) and M(3), 1.905Å) based on the observed chemical analysis and the ionic radii from Shannon (1976) for a composition of M(1) = $Li_{0.55}\square_{0.45}$ and M(2) and M(3) = $Al_{1.00}$. The radius of the vacant site was taken as 0.80 Å for this calculation. This composition for the M(1) site is in excellent agreement also with the observed scattering of 1.3 e/Å^3 at this position obtained from a Fourier difference map and the expected value of 1.4 e/Å^3. The excess of 0.044 Al in the chemical analysis (Table 1) is probably related to the uncertainty involved in the various analytical procedures, although the possibility that the excess Al enters the M(1) site cannot be ruled out.

The scattering power for each of the tetrahedral sites is: T(1), 9.5; T(11), 11.7; T(2), 11.9; and T(22), 9.1 e/Å^3. The lower scattering power and larger T—O distances for T(1) and T(22) indicate that these sites contain predominately Al and Be, whereas T(11) and T(2) are essentially Si. Actual site occupancies are impossible to calculate from this refinement because of the three possible elemental substitutions and the difficulty in obtaining an accurate ideal tetrahedral distance for Be–O (Be–O distance

Table 6. Interatomic distances and angles

Bond Lengths (Å)				Bond Angles (°)	
Octahedron M(1)					
M(1)--O(1)	2.10(3)*	O(1)--O(22)	2.775(6)	O(1)--O(22)	81(1)
O(2)	2.17(3)	O(66)	2.713(7)	O(66)	80(1)
O(6)	2.02(3)	O(2)--O(11)	2.938(6)	O(2)--O(11)	83(1)
O(11)	2.25(3)	O(66)	2.788(6)	O(66)	81(1)
O(22)	2.17(3)	O(6)--O(11)	2.778(6)	O(6)--O(11)	81(1)
O(66)	2.13(3)	O(22)	2.698(6)	O(22)	80(1)
Mean	2.14	Mean (shared)	2.782	Mean (shared)	81
		O(1)--O(2)	3.275(7)	O(1)--O(2)	100(1)
		O(6)	3.237(7)	O(6)	103(1)
		O(2)--O(6)	3.217(7)	O(2)--O(6)	100(1)
		O(11)--O(22)	3.268(7)	O(11)--O(22)	95(1)
		O(66)	3.244(7)	O(66)	96(1)
		O(22)--O(66)	3.269(7)	O(22)--O(66)	99(1)
		Mean (unshared)	3.252	Mean (unshared)	99
Octahedron M(2)					
M(2)--O(1)	1.851(5)	O(1)--O(11)	2.475(3)	O(1)--O(11)	81.1(2)
O(2)	1.933(5)	O(22)	2.775(6)	O(22)	96.5(2)
O(6)	1.903(5)	O(2)--O(22)	2.473(3)	O(2)--O(22)	81.1(2)
O(11)	1.954(5)	O(66)	2.788(6)	O(66)	93.3(2)
O(22)	1.869(5)	O(6)--O(11)	2.778(6)	O(6)--O(11)	92.1(2)
O(66)	1.902(5)	O(66)	2.356(3)	O(66)	76.5(2)
Mean	1.902	Mean (shared)	2.608	Mean (shared)	86.8
		O(1)--O(2)	2.772(6)	O(1)--O(2)	94.2(2)
		O(6)	2.741(7)	O(6)	93.8(2)
		O(2)--O(6)	2.807(8)	O(2)--O(6)	94.0(2)
		O(11)--O(22)	2.785(7)	O(11)--O(22)	93.5(2)
		O(66)	2.781(7)	O(66)	92.3(2)
		O(22)--O(66)	2.752(6)	O(22)--O(66)	93.7(2)
		Mean (unshared)	2.773	Mean (unshared)	93.6
Octahedron M(3)					
M(3)--O(1)	1.863(5)	O(1)--O(11)	2.475(3)	O(1)--O(11)	80.6(2)
O(2)	1.945(5)	O(66)	2.713(7)	O(66)	92.7(2)
O(6)	1.886(5)	O(2)--O(11)	2.938(6)	O(2)--O(11)	97.5(2)
O(11)	1.962(5)	O(22)	2.473(3)	O(22)	80.7(2)
O(22)	1.873(5)	O(6)--O(22)	2.698(6)	O(6)--O(22)	91.7(2)
O(66)	1.886(5)	O(66)	2.356(3)	O(66)	77.3(2)
Mean	1.903	Mean (shared)	2.609	Mean (shared)	86.75
		O(1)--O(2)	2.756(7)	O(1)--O(2)	92.7(2)
		O(6)	2.813(7)	O(6)	97.2(2)
		O(2)--O(6)	2.776(7)	O(2)--O(6)	92.8(2)
		O(11)--O(22)	2.750(6)	O(11)--O(22)	91.6(2)
		O(66)	2.779(7)	O(66)	92.5(2)
		O(22)--O(66)	2.776(7)	O(22)--O(66)	95.2(2)
		Mean (unshared)	2.775	Mean (unshared)	93.7
Interlayer Cation				**T(1) to T(2)**	
Ca(1)--O(3)	2.429(6)		3.406(6)	around O(3)	120.6(3)
O(4)	2.465(5)		3.538(6)	around O(4)	125.3(4)
O(5)	2.436(5)		3.381(5)	around O(5)	119.6(3)
O(33)	2.391(5)		3.414(6)	Mean	121.8
O(44)	2.446(5)		3.522(5)	**T(11) to T(22)**	
O(55)	2.423(5)		3.363(5)		
Mean (inner)	2.432	(outer)	3.437	around O(33)	119.1(3)
				around O(44)	124.3(3)
				around O(55)	119.2(3)
				Mean	120.9

Table 6. (continued)

Bond Lengths (Å)				Bond Angles (°)	
Tetrahedron T(1)				around T(1)	
T(1)--O(1)	1.728(5)	O(1)--O(3)	2.791(6)	O(1)--O(3)	108.6(3)
O(3)	1.709(6)	O(4)	2.858(6)	O(4)	112.3(3)
O(4)	1.714(6)	O(5)	2.814(6)	O(5)	108.5(3)
O(5)	1.739(6)	O(3)--O(4)	2.818(7)	O(3)--O(4)	110.9(3)
Mean	1.723	O(5)	2.802(7)	O(5)	108.7(3)
		O(4)--O(5)	2.788(8)	O(4)--O(5)	107.7(3)
		Mean	2.812	Mean	109.45
Tetrahedron T(11)				around T(11)	
T(11)-O(11)	1.624(4)	O(11)--O(33)	2.666(6)	O(11)--O(33)	109.6(3)
O(33)	1.638(5)	O(44)	2.692(6)	O(44)	111.0(3)
O(44)	1.642(5)	O(55)	2.658(6)	O(55)	109.8(3)
O(55)	1.624(6)	O(33)--O(44)	2.687(6)	O(33)--O(44)	110.0(3)
Mean	1.632	O(55)	2.646(7)	O(55)	108.4(3)
		O(44)--O(55)	2.644(7)	O(44)--O(55)	108.1(3)
		Mean	2.666	Mean	109.5
Tetrahedron T(2)				around T(2)	
T(2)--O(2)	1.644(4)	O(2)--O(3)	2.655(7)	O(2)--O(3)	109.0(3)
O(3)	1.618(6)	O(4)	2.687(6)	O(4)	110.1(2)
O(4)	1.636(5)	O(5)	2.661(7)	O(5)	109.5(3)
O(5)	1.614(6)	O(3)--O(4)	2.647(7)	O(3)--O(4)	108.9(3)
Mean	1.628	O(5)	2.632(7)	O(5)	109.0(3)
		O(4)--O(5)	2.667(7)	O(4)--O(5)	110.3(3)
		Mean	2.658	Mean	109.5
Tetrahedron T(22)				around T(22)	
T(22)-O(22)	1.712(4)	O(22)--O(33)	2.800(6)	O(22)--O(33)	108.6(3)
O(33)	1.735(5)	O(44)	2.848(6)	O(44)	112.7(2)
O(44)	1.710(5)	O(55)	2.813(6)	O(55)	109.7(3)
O(55)	1.728(6)	O(33)--O(44)	2.784(6)	O(33)--O(44)	107.8(3)
Mean	1.721	O(55)	2.787(7)	O(55)	107.2(3)
		O(44)--O(55)	2.828(7)	O(44)--O(55)	110.7(3)
		Mean	2.810	Mean	109.45

* Values in parenthesis represent estimated standard deviations (esd) in terms of the least units cited for the value to the immediate left, thus 2.10(3) indicates an esd of 0.03.

of 1.65Å according to Shannon, 1976; Be–O distance of 1.634Å according to Baur, 1981). However, two equations, one involving bond lengths and the other scattering power, may be solved simultaneously if the ideal Be–O distance is assumed to equal that of Si–O, so that there are two unknowns only. For this calculation, Si–O, Be–O and Al–O ideal distances are taken as 1.608, 1.608 and 1.771Å (Hazen and Burnham, 1973), respectively and the resulting chemical composition based on the X-ray refinement is $Ca_{1.0}Li_{0.5}\square_{0.5}Al_{2.0}$ $(Be_{0.58}Al_{1.68}Si_{1.74})O_{10}(OH)_2$ with T(1) = $Si_{0.05}Al_{0.71}Be_{0.24}$, T(11) = $Si_{0.81}Be_{0.04}Al_{0.15}$, T(2) = $Si_{0.88}Al_{0.12}$ and T(22) = $Al_{0.70}Be_{0.30}$. These results are in fair agreement with the chemical analysis (Table 1), which is not surprising in view of the discussion above and the uncertainty associated with the chemical analysis. Figure 1 illustrates the spatial relationships of the Si-rich and Al,Be-rich tetrahedra. Unlike margarite, there is no observable difference between the compositions of the two independent tetrahedral sheets.

The coupled substitutions involving the Li and Be ions reduce the lateral dimensions of both octahedral and tetrahedral sheets to a greater extent than the dimensions along either [001] or [001]* (Table 2). The octahedral sheet appears more affected than the tetrahedral sheet as suggested by the greater tetrahedral rotation angle found in the Mops mica in comparison to margarite (Table 7). This also has the result of propping apart the basal oxygen surfaces thereby increasing the interlayer separation (to 2.910Å) and elongating the octahedral coordination of the Ca ion along [001]* (ψ_{ca} = 53.25°).

Bonds from the octahedral aluminum to the undersaturated apical oxygens linked to the Al,Be-

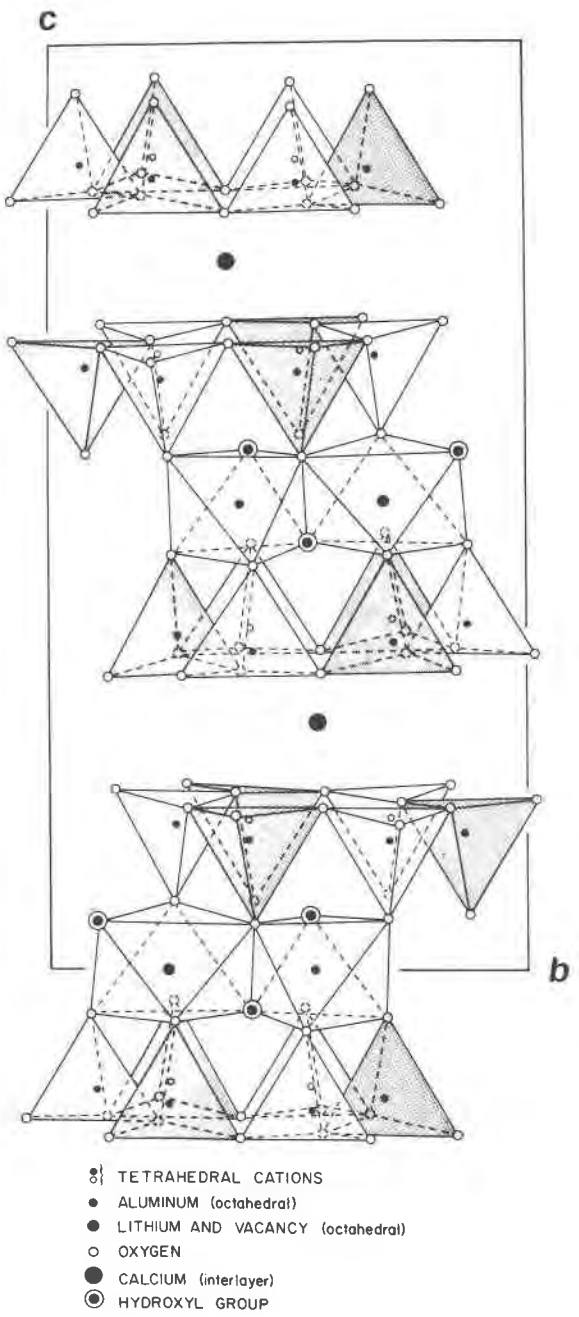

Fig. 1. Polyhedral representation of the Mops pegmatite mica X-ray structure projected down the *a* axis illustrating the tetrahedral ordering (Al,Be tetrahedra are shaded) pattern.

rich tetrahedra are significantly shorter (by approximately 0.085Å) than the bonds from the octahedral aluminum to the apical oxygens of Si-rich tetrahedra. As in margarite, aluminum octahedra avoid having either two undersaturated or two saturated apical oxygens on a shared edge.

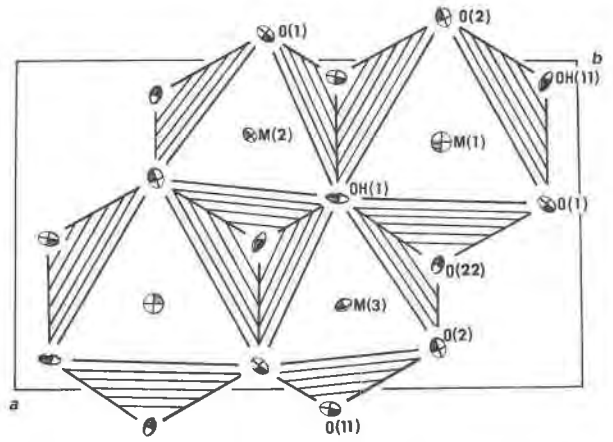

Fig. 2. Projection of the octahedral sheet on (001), showing apparent thermal vibration ellipsoids. The thermal motion of the M(1) site as illustrated has no physical significance.

Octahedral structural distortions

Comparison of the octahedral sheets of the Mops mica to that of margarite shows two significant octahedral distortions that may be attributed to the partial vacancy substitutions by lithium. One of these distortions is the counter rotation of upper and lower oxygen triads of the octahedra; the other involves the degree of the octahedral flattening as measured by the angle ψ.

Newnham (1961) recognized a counter rotation of

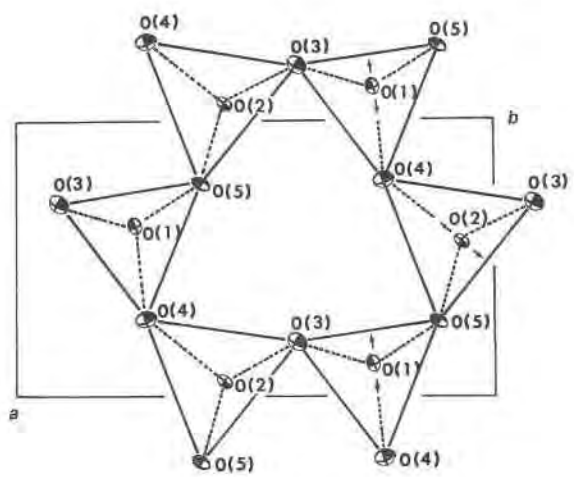

Fig. 3. Projection of the oxygen network of the tetrahedral sheet on (001), showing apparent thermal vibration ellipsoids. Arrows by O(1) and O(2) show directions in which positional deviations are expected to occur as a result of tetrahedral corrugation produced by the differing M(1) size in dioctahedral and trioctahedral unit cells.

Table 7. Structural details for the Mops mica compared to margarite

Parameter	Li, Be Mica		[4]Margarite	
[α]α_{tet} (°) = (½|120° -mean O_b-O_b-O_b angle)	[3]Sheet 1:	21.6		20.9
	Sheet 2:	21.7		20.6
[1]τ_{tet} (°) = (mean O_{apical}-T-O_{basal} angle)	Sheet 1.	T(1): 109.8		110.8
		T(2): 109.5		111.0
	Sheet 2.	T(11): 110.1		110.2
		T(22): 110.3		110.2
[β]β_{ideal} (°) = [180° - $\cos^{-1}$ (a/3c)]	95.06			95.10
[2]ψ (°) [cos ψ= oct. thickness/2(M--O,F,OH)]	Ca:	53.25		54.13
	M(1):	61.36	vacancy:	61.63
	M(2):	57.37		56.87
	M(3):	57.39		57.11
	Mean	58.71		58.54
Sheet thickness (Å) tetrahedral	Sheet 1.	2.239		2.270
	Sheet 2.	2.243		2.240
octahedral		2.051		2.080
Interlayer separation (Å)		2.910		2.876
Basal oxygen Δz_{Ave} (Å)	Sheet 1.	0.160		0.196
	Sheet 2.	0.162		0.183

1. ideal value: 109.47°
2. ideal value: 54.73°
3. sheet 1 contains T(1) and T(2), sheet 2 contains T(11) and T(22)
4. data from Guggenheim and Bailey (1977)

upper and lower oxygen triads (see Fig. 4) of the M(2) octahedron in dioctahedral layer silicates and attributed such distortions to cation-to-cation repulsions. More specifically, Radoslovich (1963) suggested that shortened shared edges produce such rotations. In 1978, Appelo defined the rotation angle, ω, to describe such rotations as the deviation from 30° of the Al–Al–O angle in plan. In margarite, the octahedral rotation angle for each aluminum octahedron is 7.4°, and in the Mops mica it is 6.2°. Such a relationship suggests that ω increases as M(1) increases in size with respect to M(2) and M(3). For 26 recently published refinements in which M(1) is larger than M(2), a plot of ω versus the ratio of the sizes of M(1) to M(2) produces a correlation coefficient for the linear regression of 99.56% (and a high level of confidence at the 0.01% level) indicating that ω of the M(2) site linearly increases as the difference between the sizes of M(1) and M(2) increases. Implicitly, octahedral cation charges and shortened shared edges are important insofar as they affect the sizes of the octahedra. Based on this regression analysis the empirical formula for ω for M(2), or M(3), and the misfit between M(1) and either M(2) or M(3) is:

$$W_e = -49.365 + 49.317 \times MF$$

where W_e is the empirically derived angle and MF is the misfit parameter, the latter being the ratio of the mean M(1)—O,OH,F distance to the mean M(2)—O,OH,F distance.

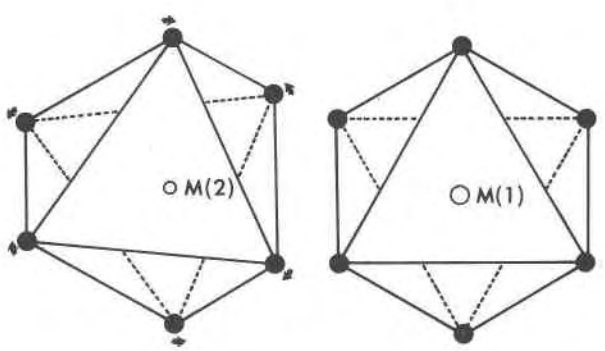

Fig. 4. Counter rotation of upper and lower oxygen triads of the octahedra are illustrated for the M(1) site (ω = 0°) and for the M(2) site (ω = 6.2°).

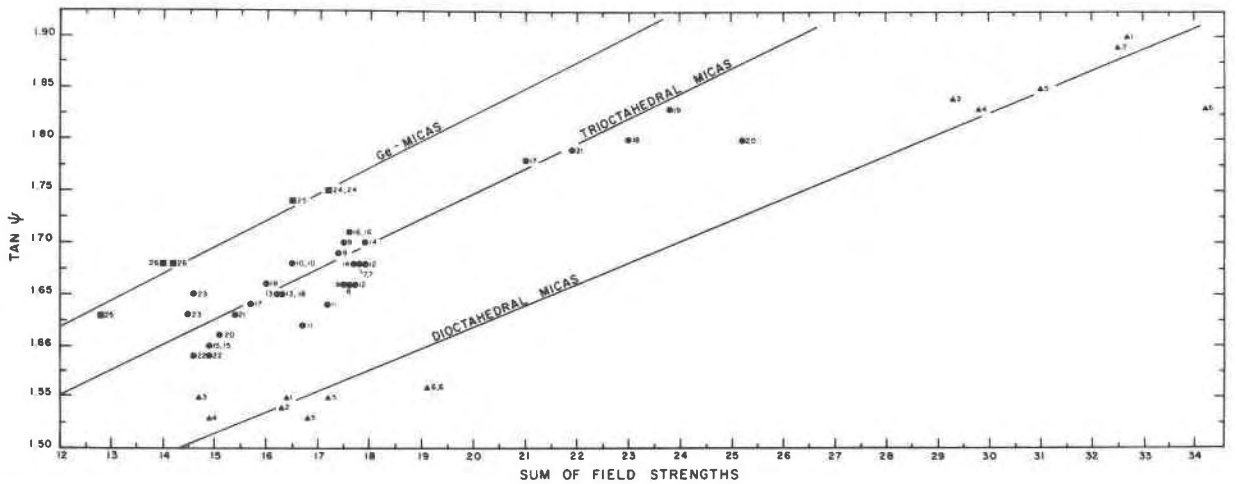

Fig. 5. Plot of tan ψ against the sum of the field strengths of neighboring octahedra. Sheet misfit, TM, is given in listing below. Squares, circles and triangles are for germanite, trioctahedral and dioctahedral micas, respectively. (1) Rothbauer, 1971, 1.08; (2), (3) Guven, 1971, muscovite: 1.08, phengite: 1.07; (4) Zhoukhilistov *et al.*, 1973, 1.07; (5) Guggenheim and Bailey, 1978, 1.12; (6) this study, 1.13; (7) Joswig, 1972, 1.07; (8) Hazen and Burnham, 1973, phlogopite: 1.07; (9) Rayner, 1974, 1.07; (10) Donnay *et al.*, 1964, 1.07; (11) Hazen and Burnham, 1973, annite: 1.05; (12) Takeda *et al.*, 1975, biotite-$2M_1$: 1.07; (13) Toraya *et al.*, 1978b, 1.05; (14) Takeda *et al.*, 1975, biotite-1M: 1.07; (15) Toraya *et al.*, 1976, 1.05; (16) McCauley *et al.*, 1973, 1.07; (17) Swanson and Bailey, 1981, 1.08; (18), (19) Guggenheim, 1981, lepidolite-$2M_2$: 1.08, 1M: 1.08; (20) Takeda *et al.*, 1971, 1.07; (21) Takeda *et al.*, 1969, 1.07; (22) Toraya *et al.*, 1977, 1.05; (23) McCauley *et al.*, 1973, 1.07; (24) Toraya *et al.*, 1978c, 1.12; (25), (26) Toraya *et al.*, 1978a, Li-poor mica: 1.11, Li-rich mica: 1.11.

Several mechanisms have been suggested for the cause of octahedral flattening, which is described by the angle (ψ) between a line drawn perpendicular to the basal plane and a line joining opposite apices of an octahedron (Donnay *et al.*, 1964). Hazen and Wones (1972) have suggested that octahedral flattening is, in part, a function of the octahedral cation radius. Since M(2) and M(3) are aluminum-rich octahedra in both the Mops mica and in margarite, the ψ angles for each octahedron should be the same. However, the values for the M(2) and M(3) octahedra for the Mops mica are 57.37° and 57.39°, and 56.87° and 57.11° for M(2) and M(3) of margarite. There is, thus, a greater degree of M(2) and M(3) flattening in the lithium-rich mica, which suggests that the neighboring octahedral occupancy of M(1) may influence the value of ψ. This evidence supports the conclusions of McCauley *et al.* (1973) that octahedral flattening is caused by the shortening of shared edges with respect to unshared edges because of cation–cation repulsions. Another cause for octahedral flattening, the partial increasing of the lateral dimensions of a smaller octahedral sheet so that it may mesh to a larger tetrahedral sheet, was suggested by Radoslovich and Norrish (1962) and confirmed by Toraya *et al.* (1978c) in a study of germanate micas.

In order to determine the relationship between octahedral flattening and both the effect of neighboring cations and the difference in octahedral/tetrahedral lateral dimensions, a multiple regression analysis involving 26 refinements was used to establish an equation relating tan ψ to two parameters. These two parameters are: (1) the sum of the field strengths, FS (*i.e.*, the ratio of valence to cation radius) of *neighboring* octahedra and (2) TM, which reflects the difference between the ideal lateral dimensions of the unrestrained tetrahedral and octahedral sheets. The latter parameter, assuming regular octahedra and tetrahedra and $\alpha = 0°$ (see Table 7 for the definition of α) is given by TM = $(4D_t)/(3D_o)$, where D_t and D_o are refined values for the tetrahedral and octahedral bond lengths (see McCauley and Newnham, 1971). Figure 5 shows that tan ψ, which is equal to the ratio between the octahedral thickness and its lateral dimension, increases as the surrounding field strength increases. Dioctahedral, trioctahedral and germanate micas were considered separately. The scatter of points, particularly for the trioctahedral micas, is related, in part, to assumptions of cation site occupancy required to calculate field strength. The analyses for both trioctahedral and germanate micas shows that tan ψ depends significantly on the neighboring field

Table 8. Orientations and magnitudes of the apparent atomic vibration ellipsoids relative to crystal axes

Atom	Axis	rms (Å) displacement	Angle (°) with respect to X	Y	Z
Ca(1)	r_1	0.091(1)[1]	93(1)	86(3)	5(3)
	r_2	0.131(2)	156(13)	114(13)	86(2)
	r_3	0.139(2)	114(13)	25(12)	93(3)
M(2)	r_1	0.060(6)	133(14)	46(27)	100(37)
	r_2	0.066(5)	96(29)	114(34)	153(22)
	r_3	0.081(5)	136(12)	126(12)	65(15)
M(3)	r_1	0.056(6)	146(10)	112(8)	60(12)
	r_2	0.078(5)	113(15)	100(28)	150(12)
	r_3	0.085(5)	114(15)	24(16)	88(26)
T(1)	r_1	0.066(7)	129(21)	116(3)	46(20)
	r_2	0.079(7)	134(20)	91(11)	130(21)
	r_3	0.134(4)	109(4)	26(3)	71(4)
T(11)	r_1	0.01(2)	109(5)	38(8)	57(10)
	r_2	0.051(5)	99(8)	60(9)	147(10)
	r_3	0.077(5)	22(6)	68(6)	93(7)
T(2)	r_1	0.052(5)	84(12)	94(5)	12(10)
	r_2	0.068(5)	165(6)	104(4)	80(12)
	r_3	0.111(3)	103(4)	14(4)	83(3)
T(22)	r_1	0.02(2)	107(6)	18(6)	93(8)
	r_2	0.076(5)	83(18)	93(8)	177(8)
	r_3	0.088(6)	19(9)	72(6)	90(19)
O(1)	r_1	0.04(1)	104(19)	87(15)	10(23)
	r_2	0.062(9)	41(12)	128(9)	80(24)
	r_3	0.100(7)	53(9)	38(9)	87(6)
O(11)	r_1	0.03(1)	96(12)	104(5)	14(5)
	r_2	0.070(9)	169(9)	80(9)	88(12)
	r_3	0.108(7)	81(8)	17(6)	77(5)
O(2)	r_1	0.063(8)	78(13)	70(23)	27(12)
	r_2	0.078(9)	63(15)	149(20)	80(23)
	r_3	0.104(7)	150(13)	112(13)	65(8)
O(22)	r_1	0.05(1)	107(10)	145(12)	58(13)
	r_2	0.080(7)	98(27)	119(16)	148(13)
	r_3	0.092(8)	19(16)	108(18)	93(23)
O(3)	r_1	0.073(9)	75(13)	121(7)	38(12)
	r_2	0.101(8)	34(13)	108(14)	122(13)
	r_3	0.126(8)	61(13)	37(9)	73(9)
O(33)	r_1	0.05(1)	133(7)	123(17)	57(13)
	r_2	0.071(9)	78(13)	141(16)	128(14)
	r_3	0.122(7)	45(5)	108(6)	55(6)
O(4)	r_1	0.074(9)	55(11)	90(8)	40(11)
	r_2	0.104(8)	42(13)	64(17)	125(13)
	r_3	0.124(8)	111(14)	26(17)	74(12)
O(44)	r_1	0.06(1)	88(16)	147(7)	58(7)
	r_2	0.087(8)	176(13)	94(15)	87(14)
	r_3	0.112(7)	94(13)	57(7)	33(7)
O(5)	r_1	0.065(9)	40(13)	110(9)	62(17)
	r_2	0.086(7)	64(16)	110(12)	150(17)
	r_3	0.113(7)	62(8)	28(9)	99(11)
O(55)	r_1	0.069(9)	53(47)	72(42)	48(24)
	r_2	0.075(8)	48(45)	135(25)	108(40)
	r_3	0.115(7)	116(7)	130(8)	48(7)
O(6)= OH	r_1	0.05(1)	31(22)	83(11)	65(20)
	r_2	0.07(1)	59(23)	113(8)	144(17)
	r_3	0.122(7)	84(6)	24(7)	114(7)
O(66)= OH	r_1	0.04(2)	126(6)	132(12)	59(12)
	r_2	0.08(1)	77(10)	133(13)	136(12)
	r_3	0.121(8)	39(6)	108(7)	62(8)

[1] Values in parenthesis represent estimated standard deviations (esd) in terms of the least units cited for the value to the immediate left, thus 0.091(1) indicates an esd of 0.001.

strengths and the effect of tetrahedral/octahedral misfit (at the 0.01% significance level) with a correlation coefficient of 96.18%. For the trioctahedral silicate micas, the empirical equation is:

$$\tan \psi = -0.0803 + 0.0201\Sigma FS + 1.3181TM$$

where ΣFS and TM are the sum of the neighboring field strengths and the misfit parameter, respectively. For dioctahedral micas, tan ψ depends only on the field strength (correlation coefficient of 98.07%, significance level of 0.01%) and the empirical equation is:

$$\tan \psi = 1.213 + 0.020\Sigma FS$$

where ΣFS is defined above. These analyses suggest that field strength of neighboring octahedra is perhaps more important an influence on the magnitude of ψ than either octahedral cation size of that site or tetrahedral/octahedral sheet misfit.

Octahedral flattening and octahedral rotation act in opposition to one another. The former produces larger upper and lower triad edges, thereby increasing the lateral dimensions of the octahedral sheet. On the other hand, the net effect of the counter rotation of the upper and lower triads of an octahedron is to reduce the lateral size of the octahedral sheet. However, this effect is small for the Mops mica, reducing the *b* cell dimension by approximately 1%.

Apparent thermal vibrations

The magnitudes and orientations of the apparent atomic vibration ellipsoids are presented in Table 8 and illustrated for the octahedral sheet in Figure 2 and for the tetrahedral sheet in Figure 3. All the atoms in the asymmetric unit have *rms* displacements elongated significantly, the smallest being that of the interlayer cation with the r_3/r_1 ratio of 1.5. Both the large magnitudes of the ellipsoids and their elongations suggest that there is a contribution to the temperature factor from positional disorder as has been suggested above based on the evidence from the hydrogen positions and Fourier difference map peaks. Clearly, since localized areas are *either* dioctahedral (*i.e.*, containing vacancies) or trioctahedral (*i.e.*, containing lithium), micas with substantial vacancies in M(1) on the average must have attributes characteristic of both dioctahedral and trioctahedral micas.

Except for the hydroxyls, the apparent vibration ellipsoids of the oxygen atoms coordinating the M(2) and M(3) sites (see Figure 2) may be described approximately as elongate parallel to (001) in a direction perpendicular to a line established by the octahedral cation and that anion. Such orientations are consistent with the positional differences caused by the counter rotation of upper and lower oxygen triads between the octahedra of the dioctahedral and trioctahedral components of the crystal. Alternatively, these same anions may be described in plan as radiating away from or toward the M(1) cation, consistent with the size of M(1) varying in

its occupancy. It is interesting to note also that the apical oxygen elongations of O(1) and O(2) as shown in Figure 3 (note associated arrows) are consistent with the tetrahedral corrugation along the [1$\bar{1}$0] direction, which produces an out-of-plane tilt about, for example, the O(4) basal oxygen. An analogous situation occurs also for the other tetrahedral sheet. Basal oxygens (Fig. 3) are elongate in directions consistent with the different tetrahedral rotations expected in the dioctahedral and trioctahedral end members.

Conclusions

A mica which shows a coupled substitution with one cation found in the octahedral sheet and the other in the tetrahedral sheet offers a special opportunity to study the effect of a single substitutional variable on each of these sheets. In this regard, the lithium for vacancy substitution in the octahedral sheet produces an apparent intermediate structure between the dioctahedral and trioctahedral end members. We anticipate a similar phenomenon for lithian muscovites ("rose muscovites") in which small amounts of lithium enter the muscovite structure. However, *X*-ray refinements may not necessarily indicate the disposition of dioctahedral and trioctahedral regions. For example, domains of Li,Be-rich regions and Li,Be-poor regions may be present and would remain undetected in this study.

Although octahedral flattening adjusts the lateral octahedral sheet dimensions to coordinate with the adjacent tetrahedral sheet, flattening of a particular octahedral site cannot be predicted by determining the occupancy of that site alone. Occupancies of surrounding octahedra have a substantial impact on the distortion of that site. Indeed, distortions involving the counter-rotation of octahedral triads are also related to neighboring octahedra and involve their size differences.

Margarite is a primary or retrograde mineral of low to medium grade metamorphic regimes. In contrast, the Mops mica is either a late magmatic or hydrothermal alteration product of beryl. The similarity of the tetrahedral ordering patterns and the diverse occurrences suggest that such ordering is not environmentally induced and is a consequence of a more stable cation charge distribution.

Acknowledgments

We acknowledge with thanks Drs. M. J. Gallagher of the Institute of Geological Sciences, Edinburgh, and David Atkin of the Institute of Geological Sciences, London, for supplying us with the Zimbabwe and Ugandan samples, the Smithsonian Institute, Washington, and Harvard University, Massachusetts, for Mt. Bity samples and Dr. D. H. Garske for a Piemonte, Italy, sample. We thank also Mr. G. Harris for the microprobe analysis, and Dr. S. W. Bailey of the University of Wisconsin-Madison for reviewing the manuscript.

Portions of this work were supported by the UICC Computing Center and by the National Science Foundation under grant EAR 80-18222.

References

Albee, A. L. and Ray, L. (1970) Correction methods for electron probe microanalysis of silicates, oxides, carbonates, phosphates, and sulfates. Analytical Chemistry, 42, 1408–1414.

Appelo, C. A. J. (1978) Layer deformation and crystal energy of micas and related minerals. I. Structural models for 1M and $2M_1$ polytypes. American Mineralogist, 63, 782–92.

Baur, W. H. (1981) Interatomic distance predictions for computer simulation of crystal structures. In M. O'Keefe and A. Navrotsky, Eds., Structure and Bonding in Crystals, p. 31–52. Academic Press, New York.

Bence, A. E. and Albee, A. L. (1968) Empirical correction factors for the electron microanalysis of silicates and oxides. Journal of Geology, 76, 383–403.

Busing, W. R., Martin, K. O., and Levy, H. A. (1962) ORFLS, a Fortran crystallographic least-squares refinement program. U.S. National Technical Information Service ORNL-TM-305.

Busing, W. R., Martin, K. O., and Levy, H. A. (1964) ORFFE, a Fortran crystallographic function and error program. U.S. National Technical Information Service ORNL-TM-306.

Cromer, D. T. and Mann, J. B. (1968) X-ray scattering factors computed from numerical Hartree-Fock wave functions. Acta Crystallographica, A24, 321–324.

Donnay, G., Morimoto, N., Takeda, H. and Donnay, J. D. H. (1964) Trioctahedral one-layer micas. I. Crystal structure of a synthetic iron mica. Acta Crystallographica, 17, 1369–1381.

Farmer, V. C. and Velde, B. (1973) Effects of structural order and disorder on the infrared spectra of brittle micas. Mineralogical Magazine, 39, 282–288.

Gallagher, M. J. and Hawkes, J. R. (1966) Beryllium minerals from Rhodesia and Uganda. Bulletin of the Geological Survey of Great Britain, 25, 59–75.

Giese, R. F., Jr. (1979) Hydroxyl orientations in 2:1 phyllosilicates. Clays and Clay Minerals, 27, 213–223.

Guggenheim, S. (1981) Cation ordering in lepidolite. American Mineralogist, 66, 1221–1232.

Guggenheim, S. and Bailey, S. W. (1975) Refinement of the margarite structure in subgroup symmetry. American Mineralogist, 60, 1023–1029.

Guggenheim, S. and Bailey, S. W. (1978) The refinement of the margarite structure in subgroup symmetry; correction, further refinement, and comments. American Mineralogist, 63, 186–187.

Guven, N. (1971) Crystal structure of $2M_1$ phengite and $2M_1$ muscovite. Zeitschrift für Kristallographie, 134, 196–212.

Hazen, R. M. and Burnham, C. W. (1973) The crystal structures of one layer phlogopite and annite. American Mineralogist, 58, 889–900.

Hazen, R. M. and Wones, D. R. (1972) The effect of cation substitutions on the physical properties of trioctahedral micas. American Mineralogist, 57, 103–129.

Holzner, J. (1936) Über den anomalen Kristallban den biotite. Zeitschrift für Kristallographie 95, 435.

Joswig, W. (1972) Neutronen beugungsmessungen an einem 1M-phlogopit. Neues Jahrbuch für Mineralogie, Monatshefte, 1–11.

Kutukova, E. I. (1959) Beryllium containing margarite from the Middle Urals (in Russian). Akadamie Nauk SSSR Mineralogicheskic Toudy, 8, 128–131.

Lacroix, A. (1908) Les minéraux de filons de pegmatite à tourmaline lithique de Madagascar. Bulletin de la Société de Française et de Minéralogie, 31, 218–247.

Lipson, H. and Cochran, W. (1966) The Determination of Crystal Structures. Cornell University Press, New York.

Lenhart, P. G. (1975) An adaptable disk-oriented automatic diffractometer control program. Journal of Applied Crystallography, 8, 568–570.

McCauley, J. W. and Newnham, R. E. (1971) Origin and prediction of ditrigonal distortion in micas. American Mineralogist, 56, 1626–1638.

McCauley, J. W. and Newnham, R. E. (1973) Structure refinement of a barium mica. Zeitschrift für Kristallographie 137, 360–367.

McCauley, J. W., Newnham, R. E. and Gibbs, G. V. (1973) Crystal structure analysis of synthetic fluorophlogopite. American Mineralogist, 58, 249–254.

Newnham, R. E. (1961) A refinement of the dickite structure and some remarks on polymorphism of the kaolin minerals. Mineralogical Magazine, 32, 683–704.

Radoslovich, E. W. (1963) The cell dimensions and symmetry of layer-lattice silicates. IV. Interatomic forces. American Mineralogist, 48, 76–99.

Radoslovich, E. W. and Norrish, K. (1962) The cell dimensions and symmetry of layer-lattice silicates. I. Some structural considerations. American Mineralogist, 47, 599–616.

Rayner, J. H. (1974) The crystal structure of phlogopite by neutron diffraction. Mineralogical Magazine, 39, 850–856.

Rothbauer, R. (1971) Untersuchung eines $2M_1$-muskovits mit neutronenstrahlen. Neues Jahrbuch für Mineralogie, Monatshafte, 143–154.

Rowledge, H. P. and Hayton, J. D. (1947) Two new beryllium minerals from Londonderry. Journal and Proceedings of the Royal Society of Western Australia, 33, 45–52.

Schomaker, V. and Marsh, R. E. (1979) Some comments on refinement in a space group of unnecessarily low symmetry. Acta Crystallographica, B35, 1933–1934.

Shannon, R. D. (1976) Revised effective ionic radii and systematic studies of interatomic distances in halides and chalcogenides. Acta Crystallographica, A32, 751–767.

Strunz, H. (1956) Bityit, ein berylliumglimmer. Zeitschrift für Kristallographie, 107, 325–330.

Swanson, T. H. and Bailey, S. W. (1981) Redetermination of the lepidolite $2M_1$ structure. Clays and Clay Minerals, 29, 81–90.

Takeda, H. and Burnham, C. W. (1969) Fluor-polylithionite: a lithium mica with nearly hexagonal $(Si_2O_5)^{2-}$ rings. Mineralogical Journal (of Japan), 6, 102–109.

Takeda, H., Haga, N. and Sadanaga, R. (1971) Structural investigation of polymorphic transition between $2M_2$-, 1M-lepidolite and $2M_1$ muscovite. Mineralogical Journal (Japan), 6, 203–215.

Takeda, H. and Ross, M. (1975) Mica polytypism: dissimularities in the crystal structures of coexisting 1M and $2M_1$ biotite. American Mineralogist 60, 1030–1040.

Toraya, H., Iwai, S., Marvmo, F., Daimon, M. and Kondo, R. (1976) The crystal structure of tetrasilicic potassium fluormica, $KMg_{2.5}Si_4O_{10}F_2$. Zeitschrift für Kristallographie, 144, 42–52.

Toraya, H., Iwai, S., Marumo, F., and Hirao, M. (1977) The crystal structure of taeniolite, $KLiMg_2Si_4O_{10}F_2$. Zeitschrift für Kristallographie, 146, 73–83.

Toraya, H., Iwai, S., Marumo, F. and Hirao, M. (1978a) The crystal structures of germanate micas $KMg_{2.5}Ge_4O_{10}F_2$ and $KLiMg_2Ge_4O_{10}F_2$. Zeitschrift für Kristallographie, 148, 65–81.

Toraya, H., Iwai, S., Marumo, F., Nishikawa, T. and Hirao, M. (1978b) The crystal structure of synthetic mica $KMg_{2.75}Si_{3.5}Al_{0.3}O_{10}F_2$. Mineralogical Journal (of Japan), 9, 210–220.

Toraya, H., Shin-ichi, I. and Marumo, F. (1978c) The crystal structure of a germanate mica, $KMg_3Ge_3Al0_{10}F_2$. Mineralogical Journal (of Japan), 9, 221–230.

Zhoukhlistov, A. P. Zvyagin, B. B., Soboleva, S. V. and Fedotov, A. F. (1973) The crystal structure of the dioctahedral mica $2M_2$ determined by high voltage electron diffraction. Clays and Clay Minerals, 21, 465–470.

Manuscript received, April 6, 1982;
accepted for publication, September 7, 1982.